Synthesis and structural characterisation of new $Ru^{II}[12]aneS_4$ complexes with polypyridylic and related ligands

Teresa M. Santos,[a] Brian J. Goodfellow,[a] João Madureira,[a] Júlio Pedrosa de Jesus,[a] Vitor Félix*[a] and Michael G. B. Drew[b]

[a] *Department of Chemistry, University of Aveiro, 3810-193 Aveiro, Portugal*
[b] *Department of Chemistry, The University, Whiteknights, Reading, UK RG6 6AD*

Received (in Cambridge, UK) 9th April 1999, Accepted 9th August 1999

The reaction between *cis*-[Ru(dmso)Cl_2] (dmso = dimethylsulfoxide) and the macrocycle 1,4,7,10-tetrathiacyclododecane ([12]aneS_4) gives the complex cation [Ru([12]aneS_4)(dmso)Cl]$^+$. A new series of Ru^{II}([12]aneS_4) complexes were obtained by replacing the dmso and the chlorine ligands with polypyridylic or related monodentate ligands. Complexes with the general formula [Ru([12]aneS_4)(L)]$^{2+}$, where L = bidentate ligand: dipyridylamine (dipa); 5-phenyl-1,10-phenanthroline (5-phen); 1,10-phenanthroline-5,6-dione (5,6-dione); *o*-phenylenediamine (pda) or 4,4′-diphenyl-2,2′-dipyridyl (dbp) have been synthesised. Related complexes containing monodentate ligands, [Ru([12]aneS_4)(CH_3CN)Cl]$^+$, [Ru([12]aneS_4)(CH_3CN)$_2$]$^{2+}$ and [Ru([12]aneS_4)(ind)Cl)]$^+$ (ind = indazole) were also prepared. The complexes were characterised by NMR, UV/Vis and IR spectroscopy and their electrochemical behaviour was studied by cyclic voltammetry. The X-ray single crystal diffraction structures of the complexes [Ru([12]aneS_4)(dmso)Cl]Cl, [Ru([12]aneS_4)(CH_3CN)$_2$][PF_6]$_2$, [Ru([12]aneS_4)(CH_3CN)Cl]PF_6, [Ru([12]aneS_4)(5,6-dione)][PF_6]$_2$·2CH_3CN, [Ru([12]aneS_4)(5-phen)][PF_6]$_2$ and [Ru([12]aneS_4)(ind)Cl]PF_6·CH_3CN were determined. All complexes exhibit a distorted *cis*-octahedral environment with the macrocycle adopting a folded conformation.

Introduction

In recent years, considerable attention has been devoted to the molecular design of transition metal polypyridyl complexes capable of selectively binding to nucleic acids.[1] In this context, Ru(II) complexes have been shown to be promising, motivating intensive research into the chemistry of Ru–polypyridyl complexes. The stabilisation of the Ru(II) oxidation state can be facilitated using macrocyclic ligands containing sulfur donor atoms. The use of these macrocyclic ligands in transition metal chemistry has been widespread in recent years, and include N (polyaza), S (polythia) and mixed N,S donors.[2] Their utility lies in the stability and inertness of the resultant complexes.[3]

The combination of macrocycles containing sulfur and nitrogen-donating polypyridyl ligands lead to stable Ru(II) complexes which can be used as ideal mimetic models for the study of the interaction of transition metal complexes with DNA. Searching for metal systems with potential DNA intercalative properties, the synthesis, structural characterisation and electrochemical behaviour of a new series of Ru(II) thioether [12]aneS_4 complexes containing polypyridylic ligands (see Scheme 1) is reported.

The most suitable method for the preparation of these compounds was found to involve, as a first step, the synthesis of the intermediate complex [Ru([12]aneS_4)(dmso)Cl]Cl **1** and subsequent replacement of Cl^- and dmso by two nitrogen donor atoms of a polypyridyl ligand in the Ru co-ordination sphere.[4,5] The intermediate complex was found to be labile to substitution by acetonitrile leading to the complex [Ru([12]aneS_4)(CH_3CN)$_2$][PF_6]$_2$ **2**. Furthermore, under mild conditions, dmso in complex **1** is found to be replaced, selectively, by monodentate ligands such as CH_3CN and indazole giving the metal complexes [Ru([12]aneS_4)(CH_3CN)Cl]PF_6 **3** and [Ru([12]aneS_4)(ind)Cl]PF_6 **4** respectively. Complexes **1**–**5** and **10** were structurally characterised by X-ray single crystal diffraction analysis.

For simplicity all complex cations reported in Scheme 1 and their corresponding neutral species are labelled with equivalent numbers.

Results and discussion

The reaction between *cis*-[Ru(dmso)$_4$$Cl_2$] and [12]ane$S_4$ produces the complex [Ru([12]aneS_4)(dmso)Cl]Cl **1**, which has proved to be a useful starting material for the synthesis of all the complexes reported here. The FTIR spectrum for complex **1** exhibits strong bands for the S=O (1076 cm^{-1}) and Ru–S stretches (424 cm^{-1}) that are similar to those seen in the related complex [Ru([9]aneS_3)(dmso)Cl_2] (1095 and 423 cm^{-1} respectively).[6] Characterisation by NMR indicated a peak at δ 3.15 (6H) from the co-ordinated dmso and a number of multiplets between δ 3.95 and 2.70 (16H) from the [12]aneS_4 ligand. The single crystal X-ray determination of the complex cation as its hexafluorophosphate salt confirms these assignments. The structure consists of discrete [Ru([12]aneS_4)(dmso)Cl]$^+$ cations and PF_6^- anions localised on the crystallographic mirror planes in the unit cell. The molecular structure of the complex cation with atomic labelling scheme is shown in Fig. 1. The ruthenium centre shows a distorted *cis*-octahedral geometry. Two sulfur atoms of the macrocyclic ligand, one chlorine and one sulfur atom from the dmso ligand define the equatorial plane. Two remaining sulfur donor atoms of the macrocyclic ligand occupy the axial octahedral positions. Selected bond lengths and angles in the Ru co-ordination sphere are listed in Table 1.

A differential *trans* influence for Cl and dmso is apparent from the values of the Ru–S bond lengths in the equatorial plane. The Ru–S(7) bond length [2.278(2) Å], *trans* to the Cl ligand, is 0.074 Å shorter than the Ru–S(1) bond length

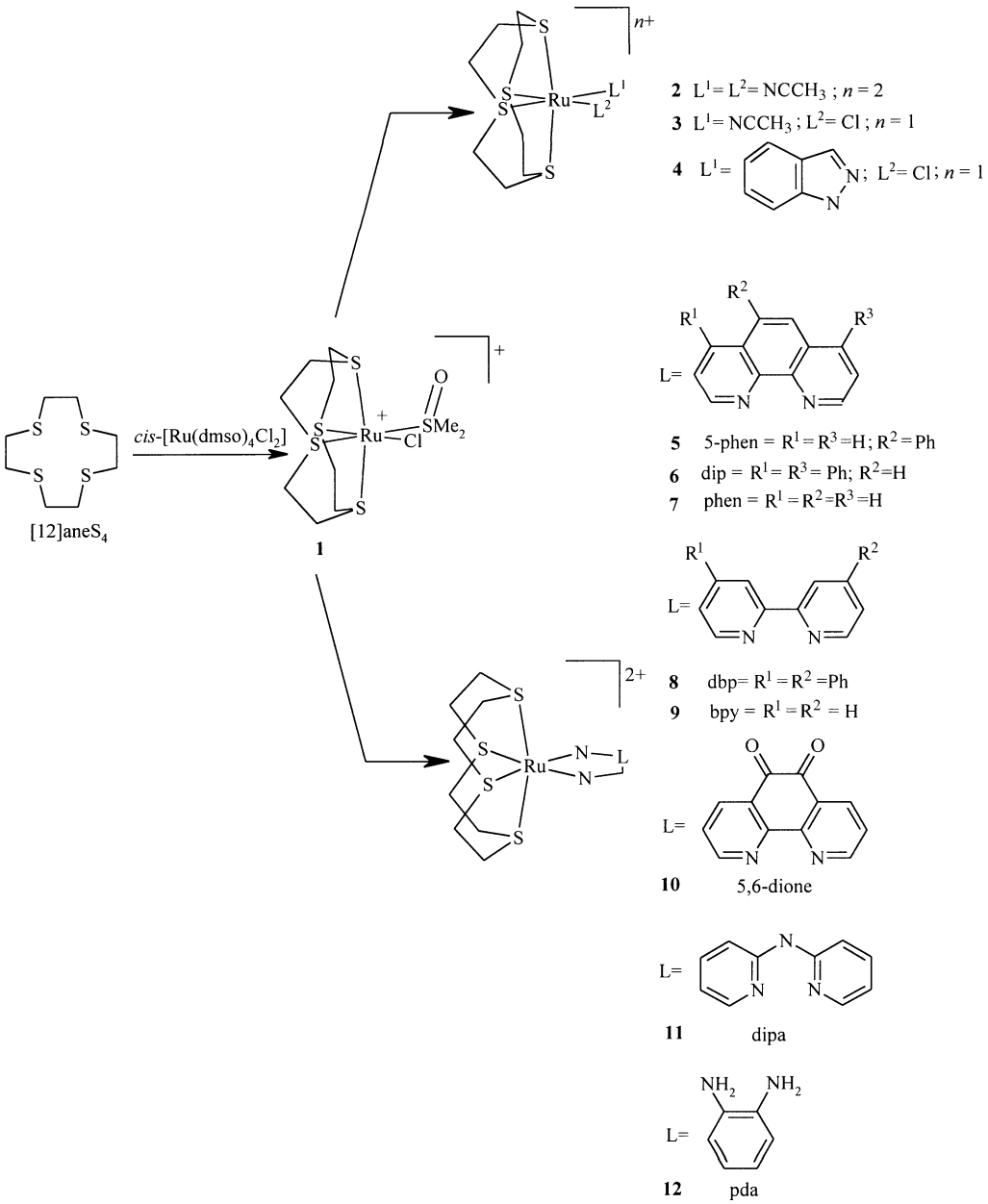

Scheme 1

[2.352(3) Å], which is *trans* to the sulfur donor S(8) from the dmso ligand. The Ru–S(8) [2.291(3) Å] and Ru–Cl [2.441(3) Å] equatorial bond lengths are similar to those found for the octahedral complex [Ru([9]aneS$_3$)](dmso)Cl$_2$], where the dmso and Cl ligands are mutually *trans* and therefore show a *trans* effect with a similar magnitude [Ru–Cl 2.444(2) and Ru–S 2.287(2) Å].[6] The range of the bond angles subtended at S(8), 99.4(2)° to 119.65(15)°, indicate a distorted tetrahedral stereochemistry for the dmso ligand.

Table 1 Selected bond lengths (Å) and angles (°) for cation **1**

Ru–S(8)	2.291(3)	Ru–Cl	2.441(3)
Ru–S(7)	2.278(2)	Ru–S(1)	2.352(3)
Ru–S(4)	2.367(3)		
S(8)–Ru–Cl	87.64(5)	S(4)–Ru–S(4*)	166.38(5)
S(4)–Ru–Cl	92.68(2)	S(7)–Ru–Cl	178.00(4)
S(7)–Ru–S(8)	90.36(6)	S(7)–Ru–S(1)	92.06(4)
S(7)–Ru–S(4)	87.54(2)	S(8)–Ru–S(1)	177.58(3)
S(8)–Ru–S(4)	96.36(2)		
O(81)–S(8)–Ru	119.65(15)	C(92)–S(8)–Ru	110.78(12)
O(81)–S(8)–C(92)	107.14(15)	C(92*)–S(8)–C(92)	99.4(2)

* Symmetry element: $x, -y + 3/2, z$.

Complex **3** was obtained by dissolving complex **1** in CH_3CN and eluting the resultant solution through an anion exchange column (QAE Sephadex A-25 column, Cl^- form, eluent CH_3CN). The FTIR spectrum of this complex displays the characteristic C≡N stretching bands of the co-ordinated CH_3CN at 2320 and 2282 cm^{-1} and the Ru–Cl stretch at 266 cm^{-1}. The NMR spectrum shows a singlet at δ 1.97 (3H) for the co-ordinated CH_3CN ligand.

Reflux of complex **1** in CH_3CN in presence of $TlPF_6$ afforded complex **2**. Treatment of complex **3** under the same reaction conditions also produced complex **2**. It was found that without $TlPF_6$ complex **2** could not be produced directly by refluxing complexes **1** or **3** in CH_3CN. These results suggest that the reaction requires the Tl salt to remove the chloride and allow substitution of the dmso ligand in the ruthenium(II) co-ordination sphere. Similar behaviour was found for the reaction of [Ru([9]aneS$_3$)(dmso)Cl$_2$] with CH_3CN where $Ag(CF_3SO_3)$ was required to produce [Ru([9]aneS$_3$)(CH$_3$CN)$_3$]$^{2+}$.[6] The C≡N stretching bands in

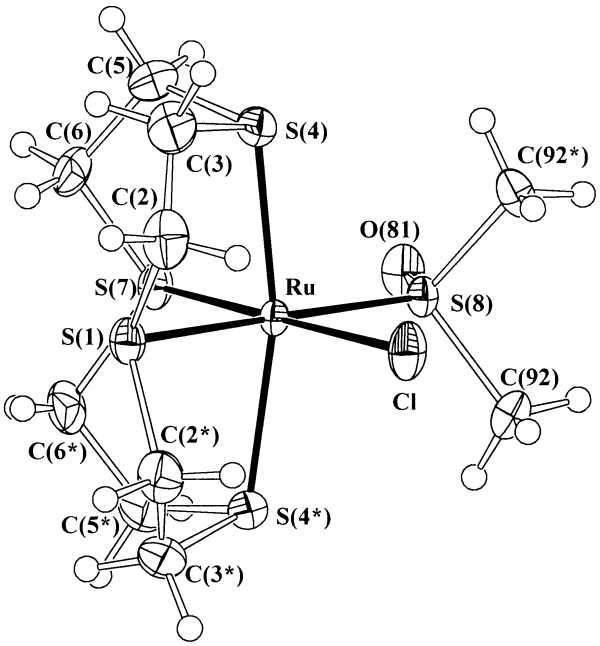

Fig. 1 Molecular structure of the $[Ru([12]aneS_4)(dmso)Cl]^+$ cation **1** with the labelling scheme adopted. Thermal ellipsoids are drawn at the 40% probability level.

the FTIR spectrum of complex **2** occur at 2322, 2289 and 2254 cm^{-1}, and the typical Ru–Cl stretching frequency present in complex **3** disappears. The ^1H NMR spectrum of **2** shows two separate resonances for the co-ordinated CH_3CN ligand. The ^{13}C NMR spectrum of **2** displays four resonances between δ 45 and 30 from the $[12]aneS_4$ carbon atoms indicating C_{2v} symmetry.

The experimental observation that a $TlPF_6$ salt is required for substitution of the Cl^- and dmso ligands to produce complex **2** suggests that, in the reaction to produce the mono-substituted CH_3CN complex **3**, the resin plays an important role. A possible mechanism to produce complex **3** could involve substitution of the dmso ligand by Cl^- from the resin leading to an intermediate with two bound Cl^- ligands. In order to preserve the charge balance of the resin one Cl^- is replaced, on elution, by a CH_3CN molecule from the eluent.

The molecular structures of complexes **2** and **3** were definitively established by single crystal X-ray diffraction determinations. The asymmetric unit of complex **2** consists of one disordered $[Ru([12]aneS_4)(CH_3CN)_2]^{2+}$ cation, two PF_6^- anions and one solvent of crystallisation molecule (CH_3CN) located in general crystallographic positions. The disordered model found for the macrocyclic ligand leads to two different conformational isomers for the metal complex in the solid state. Fig. 2 shows the molecular structure of the complex cation **2** determined by the macrocyclic conformation with major occupancy in the unit cell.

The asymmetric unit of complex **3** comprises a discrete $[Ru([12]aneS_4)(CH_3CN)Cl]^+$ cation and a PF_6^- anion localised on a crystallographic mirror plane. The fluorine atoms are disordered over two alternative positions in the unit cell.

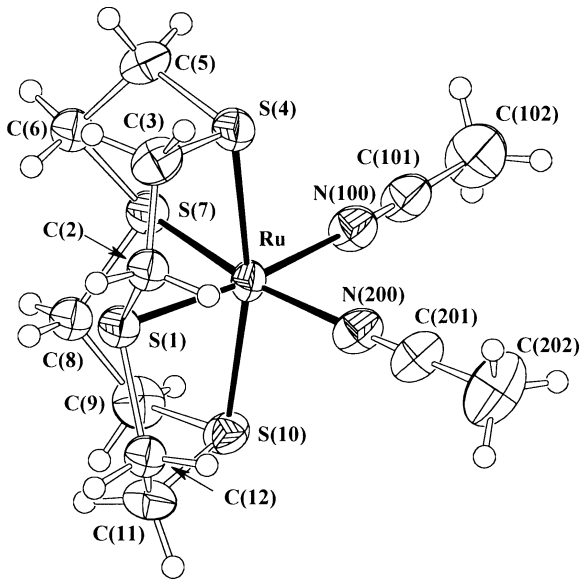

Fig. 2 Molecular structure of the $[Ru([12]aneS_4)(CH_3CN)_2]^{2+}$ cation **2** with labelling scheme adopted. Thermal ellipsoids are drawn at the 40% probability level.

Table 2 Selected bond lengths (Å) and angles (°) for cations **2**[a] and **3**

Cation **2**			
Ru–N(100)	2.086(6)	Ru–N(200)	2.055(7)
Ru–S(1)	2.239(4), *2.401(5)*	Ru–S(7)	2.362(3), *2.220(5)*
Ru–S(4)	2.362(2)	Ru–S(10)	2.363(2)
N(200)–Ru–N(100)	89.7(2)	S(4)–Ru–S(10)	167.6(1)
N(100)–Ru–S(1)	170.9(2), *166.5(2)*	N(100)–Ru–S(4)	94.1(2)
N(100)–Ru–S(7)	79.3(2), *102.7(2)*	N(100)–Ru–S(10)	95.2
N(200)–Ru–S(1)	99.4(2), *76.8(2)*	N(200)–Ru–S(10)	94.3(2)
N(200)–Ru–S(4)	94.1(2)	N(200)–Ru–S(7)	169.0(2), *167.6(2)*
S(1)–Ru–S(4)	84.9(1), *86.1(1)*	S(1)–Ru–S(7)	91.6(2), *90.8(2)*
S(1)–Ru–S(10)	84.6(1), *86.9(1)*	S(4)–Ru–S(7)	86.5(1), *85.2(1)*
S(7)–Ru–S(10)	87.01(9), *84.7(1)*		
C(101)–N(100)–Ru	177.4(6)	C(201)–N(200)–Ru	177.7(6)
N(100)–C(101)–C(102)	179.0(9)	N(200)–C(201)–C(202)	179.3(9)
Cation **3**			
Ru–N(100)	2.070(16)	Ru–Cl	2.462(4)
Ru–S(1)	2.284(5)	Ru–S(4)	2.356(2)
Ru–S(7)	2.272(4)		
N(100)–Ru–Cl	88.2(5)	S(4)–Ru–S(4*)	167.2(1)
N(100)–Ru–S(1)	179.3(5)	N(100)–Ru–S(4)	95.71(8)
N(100)–Ru–S(7)	86.8(5)	S(1)–Ru–Cl	92.5(2)
S(4)–Ru–Cl	93.01(8)	S(7)–Ru–Cl	175.0(2)
S(1)–Ru–S(4)	84.3(1)	S(7)–Ru–S(1)	92.5(2)
C(101)–N(100)–Ru	174.2(13)	N(100)–C(101)–C(102)	175.0(9)

[a] The italic values reported for cation **2** refer to the minor component of the disorder present in the crystal lattice.
* Symmetry operation: $x, -y, z$.

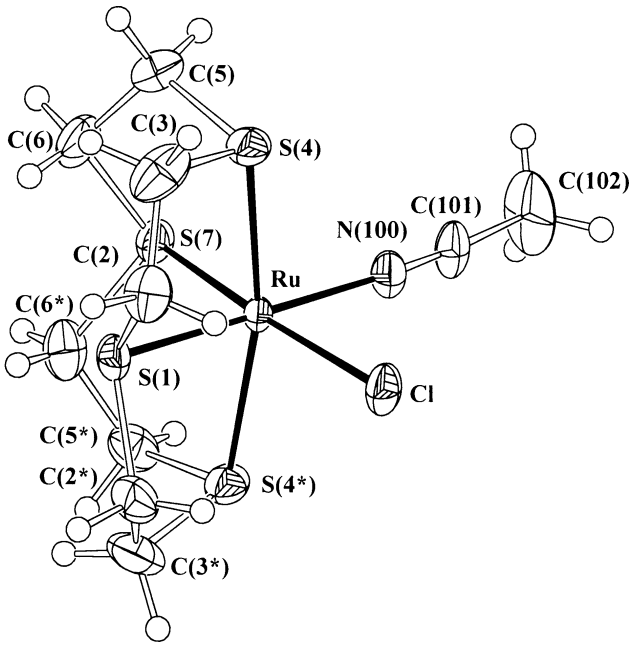

Fig. 3 Molecular structure of the $[Ru([12]aneS_4)(CH_3CN)Cl]^+$ cation **3** with labelling scheme adopted. Thermal ellipsoids are drawn at the 40% probability level.

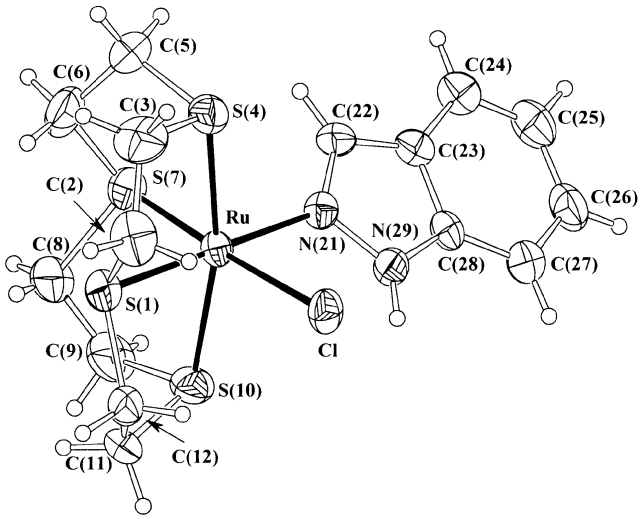

Fig. 4 Molecular structure of the $[Ru([12]aneS_4)(ind)Cl]^+$ cation **4** with labelling scheme adopted. Thermal ellipsoids are drawn at the 40% probability level.

Fig. 3 displays the molecular structure of the complex cation **3** with the atomic labelling scheme adopted.

The structural parameters associated with the ruthenium co-ordination spheres of complexes **2** and **3**, listed in Table 2, indicate a distorted *cis*-octahedral geometry for both complexes. The equatorial planes comprise two macrocyclic sulfurs and two donor atoms of monodentate ligands: two nitrogens from CH_3CN ligands in complex **2** and one nitrogen from CH_3CN and one chlorine in complex **3**. Six-co-ordination is achieved *via* the two remaining sulfur donor atoms of the macrocyclic ligand.

Detailed analysis of the equatorial Ru–S bond lengths for complex **2** is precluded by the disorder found in the macrocyclic ligand. The best trial model found to account for the disorder comprises two alternative sites for the sulfur donor atoms S(1) and S(7) leading to two different values for each of the equatorial Ru–S bond lengths [Ru–S(1) 2.239(4) and 2.401(5) Å and Ru–S(7) 2.362(3) and 2.220(5) Å]. The pattern of equatorial bond lengths, found for complex **3**, indicate a slight *trans* effect. The Ru–S(7) bond [2.272(4) Å], *trans* to the Ru–Cl bond, is shorter than the Ru–S(1) bond [2.284(5) Å] *trans* to the Ru–N bond. The two complexes have similar Ru–N bond lengths [2.070(16) Å in **3** and on average 2.071(7) Å in **2**]. The Ru–N–C angles of 177.4(6) and 177.7(6)° in **2** and 174.2(13)° in **3** show that the CH_3CN ligands in both cases are, as expected, bonded linearly to the ruthenium centre.

The other monodentate ligand, indazole, was introduced easily into the ruthenium co-ordination sphere, replacing the dmso ligand. The difficulties found in the preparation of the CH_3CN complexes **2** and **3** did not occur in the synthesis of complex **4** due to the differing co-ordination properties of the two ligands. CH_3CN and indazole are both π acceptors but display differing σ donor abilities.[7] The indazole nitrogen has greater nucleophilic character than the nitrogen donor of CH_3CN and therefore attacks the ruthenium centre more easily.

The X-ray diffraction analysis of complex **4** shows that its crystal structure is built up from an asymmetric unit containing one $[Ru([12]aneS_4)(ind)Cl]^+$ cation, one PF_6^- anion and one CH_3CN solvent of crystallisation molecule localised in general positions. The PF_6^- anions are disordered over two positions in the crystal lattice. Fig. 4 displays the molecular structure of the complex cation **4** together with the labelling scheme used. This cation has a distorted *cis*-octahedral geometry with the equatorial plane formed by two macrocyclic sulfurs, one chlorine and one nitrogen from the indazole ligand. The axial positions are occupied by the remaining two macrocyclic sulfur donor atoms. Selected bond lengths and angles are given in Table 3.

The indazole ligand is tilted by 41.0(2)° relative to the least squares plane determined by the atoms S(1), S(7), Cl and N(21). This relative orientation may be the result of a delicate balance between the minimisation of the steric interactions of Cl and the indazole ring and the electronic requirements of the Ru(II) centre, which lead to a N(21)–Ru–Cl angle of 87.1(2)°.

The equatorial bond lengths indicate that the *trans* effect is also present in complex **4**, but is less pronounced than that reported for complex **1**. The Ru–S(1) bond [2.316(3) Å], *trans* to the Ru–N bond, is only 0.046 Å longer than the Ru–S(7) bond [2.270(3) Å], which is *trans* to the Ru–Cl bond. The Ru–N(21) bond length [2.101(7) Å] is similar to those found for polypyridylic complexes **5** and **10** (see Table 4 below) suggesting the nitrogen donors of the ind, 5-phen and 5,6-dione ligands have comparable co-ordination proprieties. In contrast, both complexes **2** and **3**, which contain CH_3CN ligands, show shorter Ru–N bonds and therefore display different co-ordination abilities.

The synthesis of the bidentate polypyridylic complexes **5**, **8**, **10**, **11** and **12**, as expected, was more straightforward due to the chelate effect. The characterisation of these complexes by ^1H NMR indicated that the expected stoichiometry was observed in all cases. A previous study of the complexes

Table 3 Selected bond lengths (Å) and angles (°) for cation **4**

Ru–N(21)	2.101(7)	Ru–Cl	2.448(2)
Ru–S(1)	2.316(3)	Ru–S(4)	2.363(3)
Ru–S(7)	2.270(3)	Ru–S(10)	2.352(3)
N(21)–Ru–Cl	87.1(2)	S(10)–Ru–S(4)	167.1(1)
N(21)–Ru–S(1)	179.6(2)	N(21)–Ru–S(4)	96.1(2)
N(21)–Ru–S(7)	87.2(2)	N(21)–Ru–S(10)	95.5(2)
S(1)–Ru–Cl	92.5(1)	S(4)–Ru–Cl	93.9(1)
S(7)–Ru–Cl	174.3(1)	S(10)–Ru–Cl	92.5(1)
S(1)–Ru–S(4)	84.0(1)	S(1)–Ru–S(10)	84.5(1)
S(7)–Ru–S(1)	93.1(1)	S(7)–Ru–S(4)	87.4(1)
S(7)–Ru–S(10)	87.3(1)		

$[Ru([12]aneS_4)(dip)]^{2+}$ (dip = 4,7-diphenyl-1,10-phenanthroline) **6**, $[Ru([12]aneS_4)(phen)]^{2+}$ (phen = 1,10-phenanthroline) **7** and $[Ru([12]aneS_4)(bpy)]^{2+}$ **9** (bpy = 2,2′-bipyridyl),[5] showed broad lines in the ^1H spectra for the aromatic protons closest to the ruthenium and for the [12]aneS$_4$ CH_2 protons. The conclusion drawn was that chemical exchange was taking place, probably involving cleavage of the Ru–N bond. A similar situation is observed in the ^1H spectra of the complexes with bidentate ligands **5**, **8**, **10** and **11**. This suggests that steric crowding, due to the [12]aneS$_4$ ring and the bite angle of the polypyridyl ligand, is also occurring in these complexes which results in chemical exchange taking place in order to relieve the strain at the ruthenium centre. The ^1H NMR spectrum of complex **10** is shown in Fig. 5a. Complex **12** displays sharp lines for all the [12]aneS$_4$ protons and all the aromatic protons indicating that chemical exchange is not taking place. This complex has only one aromatic ring (pda) and therefore steric interactions between the aromatic ligand and the [12]aneS$_4$ macrocycle are avoided. Fig. 5b shows the ^1H NMR spectrum of complex **12**.

FTIR characterisation of the complexes showed typical Ru–S stretching frequencies, except for complex **11** where only very weak absorption was seen. Complex **10**, containing C=O groups in the polypyridyl ligand, shows a strong band due to the carbonyl stretch at 1699 cm^{-1}. The frequencies and the appearance of the N–H stretching bands for complex **11** (3329, 3255 and 3215 cm^{-1}) indicate that the polypyridyl-bridging N is not co-ordinated to the metal.[8] Complex **12** shows a single fairly weak band at 3228 cm^{-1}, which is typical for a primary amine. The free pda ligand has two very strong stretches at 3385 and 3364 cm^{-1}, their absence suggesting that co-ordination *via* nitrogen has occurred.

The electronic spectra of all the Ru(II) polypyridylic complexes feature a UV/Vis pattern similar to that seen for analogous Ru(II) thioether polypyridylic complexes, such as $[Ru([12]aneS_4)(bpy)]^{2+}$ **9** and $[Ru([12]aneS_4)(dip)]^{2+}$ **6**† as well as other Ru(II) complexes containing only polypyridylic or S-donor ligands.[10–14] The characteristic high energy UV intraligand $\pi \rightarrow \pi^*$ bands occur at around 200 nm and between 250 and 300 nm. Intense l.m.c.t. $(dt_{2g}) \rightarrow \pi^*$ (ligand) bands appear between 390 and 500 nm. Additionally the UV spectra show intense bands between 300 and 350 nm, although their origin is not clear. Crystal structures of complexes **5** and **10** were determined by X-ray diffraction. In the

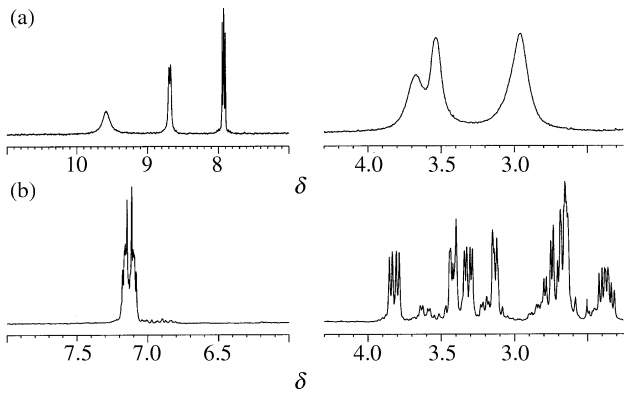

Fig. 5 (a) ^1H NMR spectrum of complex **10** showing the broadening of the proton peaks of the [12]aneS$_4$ ligand (δ 4–2) and of the peaks for the H-2/H-9 protons (δ 10–7) closest to the Ru(II) centre. (b) ^1H NMR spectrum of complex **12** showing sharp lines for all resonances.

† UV/Vis (H_2O) λ_{max} nm ($\varepsilon \times 10^{-3}$ M^{-1} cm^{-1}): $[Ru([12]aneS_4)(bpy)]^{2+}$ 408 (4.7), 313 (7.8), 294 (10.8), 264 (12.0), 207 (29.2); $[Ru([12]aneS_4)(dip)]^{2+}$ 417 (7.2), 283 (27.2), 248 (15.4), 203 (50.0)].[9]

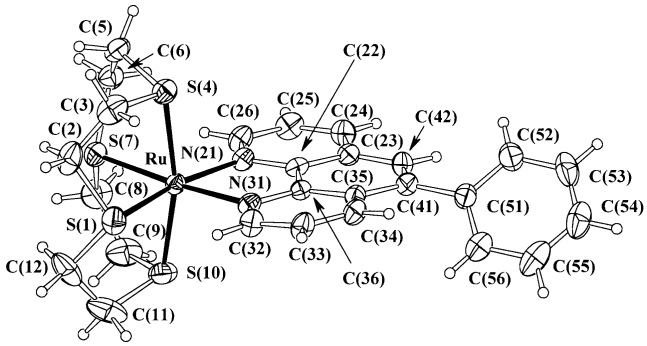

Fig. 6 Molecular structure of the $[Ru([12]aneS_4)(5\text{-phen})]^{2+}$ cation **5** with labelling scheme adopted. Thermal ellipsoids are drawn at the 40% probability level.

asymmetric unit of complex **5** there is a $[Ru([12]aneS_4)(5\text{-phen})]^{2+}$ complex cation and two PF_6^- anions in general positions. The asymmetric unit of complex **10** comprises a complex $[Ru([12]aneS_4)(5,6\text{-dione})]^{2+}$ cation on a twofold axis, and a PF_6^- anion and a CH_3CN solvent molecule in general positions. Molecular diagrams including the corresponding atomic labelling schemes are shown in Figs. 6 and 7 for complex cations $[Ru([12]aneS_4)(5\text{-phen})]^{2+}$ and $[Ru([12]aneS_4)(5,6\text{-dione})]^{2+}$ respectively. Table 4 lists selected bond lengths and angles for cations **5** and **10**. In both

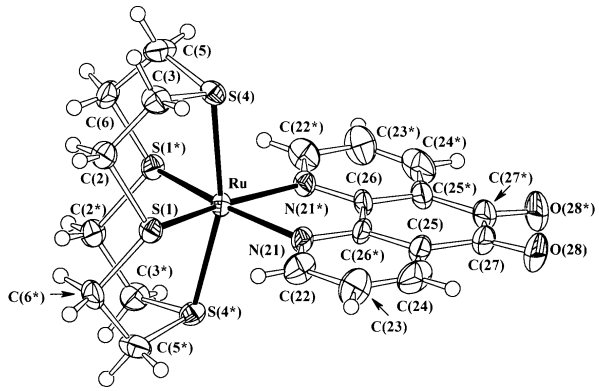

Fig. 7 Molecular structure of the $[Ru([12]aneS_4)(5,6\text{-dione})]^{2+}$ cation **10** with labelling scheme adopted. Thermal ellipsoids are drawn at the 40% probability level.

Table 4 Selected bond lengths (Å) and angles (°) for cations **5** and **10**

Cation **5**			
Ru–N(21)	2.131(4)	Ru–N(31)	2.113(4)
Ru–S(1)	2.301(1)	Ru–S(4)	2.373(2)
Ru–S(7)	2.303(2)	Ru–S(10)	2.346(2)
N(31)–Ru–N(21)	78.3(2)	S(10)–Ru–S(4)	166.5(1)
N(21)–Ru–S(1)	170.1(1)	N(21)–Ru–S(4)	96.9(1)
N(21)–Ru–S(7)	100.9(1)	N(21)–Ru–S(10)	91.1(1)
N(31)–Ru–S(1)	92.5(1)	N(31)–Ru–S(4)	92.4(1)
N(31)–Ru–S(7)	175.2(1)	N(31)–Ru–S(10)	99.9(1)
S(1)–Ru–S(4)	87.2(1)	S(1)–Ru–S(7)	88.61(8)
S(1)–Ru–S(10)	86.8(1)	S(7)–Ru–S(4)	83.02(8)
S(7)–Ru–S(10)	84.8(1)		
Cation **10**			
Ru–N(21)	2.149(5)	Ru–S(1)	2.295(2)
Ru–S(4)	2.382(2)		
N(21)–Ru–N(21*)	77.6(3)	S(4*)–Ru–S(4)	161.8(1)
N(21)–Ru–S(1)	89.4(2)	N(21)–Ru–S(1*)	166.6(1)
N(21)–Ru–S(4*)	94.6(1)	S(1*)–Ru–S(1*)	103.8(1)
S(1)–Ru–S(4*)	84.45(8)	N(21)–Ru–S(4)	99.6(1)
S(1)–Ru–S(4)	84.36(8)		

* Symmetry relation: $-x + 1, y, -z + 1/2$.

complexes the metal centre exhibits a distorted *cis*-octahedral arrangement. The equatorial planes are defined by two macrocyclic sulfurs and two nitrogen atoms from bidentate polypyridylic ligands (5-phen or 5,6-dione). The axial positions are occupied by the remaining two macrocyclic sulfur donor atoms.

The average Ru–N bond lengths of 2.122(4) Å in **5** and 2.149(5) Å in **10** are identical to those seen for other Ru^{II}[12]aneS_4 polypyridyl derivatives, such as [Ru([12]-aneS_4)(dip)]$^{2+}$ **6** [2.136(6) Å], [Ru([12]aneS_4)(phen)]$^{2+}$ **7** [2.159(6) Å] and [Ru([12]aneS_4)(bpy)]$^{2+}$ **9** [2.162(6) Å].[5] These five complexes exhibit similar N–M–N angles of 78.3(2)° in **5**, 77.6(3)° in **10**, 77.4(4)° in **6**, 79.6(3)° in **7**, and 77.9(3)° in **9**, which reflect the small bite angle of their polypyridylic ligands, 5-phen, 5,6-dione, dip, phen or bpy. In contrast, the complexes containing monodentate ligands, (complexes **1**–**4**), where this steric constraint is absent, display wider angles on the equatorial plane close to the ideal octahedral value of 90°, S–Ru–Cl 87.64(5)° in **1**, N–Ru–N 89.7(2)° in **2**, and Cl–Ru–N 88.2(5)° in **3** and 87.1(2)° in **4**.

In order to investigate the redox properties of Ru^{II}([12]aneS_4) polypyridylic systems electrochemical studies (cyclic voltammetry, CV) were carried out for complexes **5**, **8**, **10** and **11**. Table 5 also lists data for the related Ru^{II}([12]aneS^4) polypyridylic derivatives **6**, **7** and **9**. Data for [Ru([12]aneS_4)(ind)Cl]$^+$ **4** are also included in Table 5 for comparison purposes. Results indicate that, in general, all polypyridylic complexes exhibit comparable electrochemical behaviour. From the chemical point of view, although the indazole ligand is not a derivative of phen or bpy; the CV results for complex **4** compare well with those found for the polypyridylic systems.

The complexes undergo several oxidation and/or reduction processes in the potential window + 1.6 to − 1.6 V. All show similar electrochemical properties in the positive potential range, characterised by either a reversible redox wave (peak-

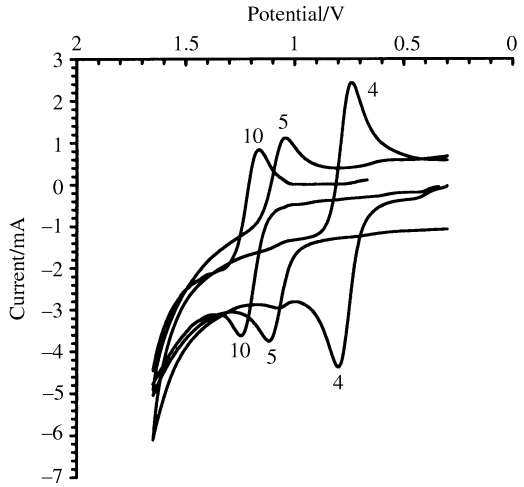

Fig. 8 Cyclic voltammograms of acetonitrile–NBu_4PF_6 solutions of complexes **4**, **5** and **10**, obtained with scan rates of 50, 100 and 200 mV s^{-1} respectively (potentials *vs.* Ag^+–AgCl reference electrode).

Table 5 Electrochemical data for complexes **4**–**11**[a]

Complex	Potentials/mV			
	E_{pa}	E_{pc}	ΔE_p	$E_{1/2}$[b]
[Ru([12]aneS_4)(ind)Cl]$^+$ **4**	1209	1144	65	1176
	1481	1429	52	1456
	−500	−72	76	−538
	—	−576	—	—
	—	−1334[b]	—	—
[Ru([12]aneS_4)(5-phen)]$^{2+}$ **5**	1522	1456	66	1489
	−1178	−1241	63	−1201
	—	1441	—	—
[Ru[12]aneS_4(dip)]$^{2+}$ **6**[c]	1108	—	—	—
	1494	—	—	—
	—	−1296	—	—
[Ru([12]aneS_4)(phen)]$^{2+}$ **7**[c]	1108	1014	94	1061
	1266	1200	66	1233
	1518	1436	82	1477
	−1207	−1266	59	−1237
	—	−1330	—	—
	—	−1514	—	—
[Ru([12]aneS_4)(dbp)]$^{2+}$ **8**	1124	—	—	—
	1494	1408	86	1451
	−1157	−1215	58	−1186
	—	−1432	—	—
[Ru([12]aneS_4)(bpy)]$^{2+}$ **9**[c]	1112	—	—	—
	1478	—	—	—
	—	−1314	—	—
	—	−1436	—	—
[Ru([12]aneS_4)(5,6-dione)]$^{2+}$ **10**	1629	1564	65	1597
	+1	−62	63	−31[d,e]
	−529	−595	66	−562[e,g]
	−524	−603	79	−566[f,g]
	−473	−605	132	—[h]
	462	−605	143	—[i]
[Ru([12]aneS_4)(dipa)]$^{2+}$ **11**	1130	1071	59	1101
	1484	—	—	—
	—	−1236	—	—

[a] All potentials are quoted relative to SSC reference electrode. [b] $E_{1/2}$ is defined as $(E_{pa} + E_{pc})/2$, where E_{pa} and E_{pc} are the anodic and cathodic electrode potentials respectively. [c] Ref. 5. [d] BQ/SQ redox wave. [e] Scan rate 100 mV s^{-1}. [f] Scan rate 100 mV s^{-1} (repetitive scanning). [g] SQ/Cat redox wave. [h] Scan rate 500 mV s^{-1}. [i] Scan rate 500 mV s^{-1} (repetitive scanning).

to-peak separations $\Delta E_p = 60$–90 mV) or by an irreversible oxidative response ($E_{1/2}$ or E_{pa} of *ca.* 1.1–1.4 V). Complex **10** is an exception (see below) with a redox wave at $E_{1/2} \approx 1.60$ V. These waves correspond to the metal-centred redox reaction usually assigned to the Ru^{3+}/Ru^{2+} couple.[11–13,15–20] Fig. 8 shows the cyclic voltammograms of complexes **4**, **5** and **10** respectively.

In general, all complexes also display, at more positive potentials, either a second reversible or a single oxidation peak (ΔE_p or $E_{pa} \approx 1.5$ V) or even a third oxidation peak at high potentials, as for example in complex **7** (Table 5). Attempts to define some of the respective anodic counterparts were unsuccessful mainly due to the poor stability of the Cl^- salts of some of the compounds. These second and third waves may be eventually explained by: (i) further metal oxidation reactions,[21,22] or (ii) the formation of co-ordinated oxidized ligands.[10,14,16,17,20] Analogous high potential irreversible oxidation peaks have been found for other Ru(II)–polypyridylic compounds, although these were measured in liquid SO_2.[18]

In complex **10**, the $E_{1/2}$ (Ru^{3+}/Ru^{2+}) ≈ 1.60 V value is shifted to a more positive potential than for the other complexes, possibly because of an increase of the nuclear charge at the ruthenium centre resulting from back-bonding to the 5,6-dione (two C=O groups resulting in higher electron-withdrawing character of this ligand with respect to other polypyridylic ligands).[15,23] A co-ordinated 5,6-dione ligand normally undergoes inter-conversion among benzoquinone (BQ), semiquinone (SQ) and catecholate (Cat) species.[23,24] As is shown in Table 5 a BQ/SQ reversible redox wave can be seen at a potential of -31 mV, independent of the experimental conditions. But, whenever a slow scan speed (100 mV s^{-1}) is used, the anodic peak associated with BQ/SQ is accompanied by a less intense second anodic peak (*ca.* -138 to -106 mV) which may correspond to a slowly formed intermediate, not observed if faster scan rates are applied. The SQ/Cat inter-conversion is strongly dependent on the scan rate. Under slower scan rates a reversible redox process ($\Delta E_p = 66$ mV; $E_{1/2} = -562$ mV) can be considered, although the E_{pa} peak does not appear to be very well defined. If a slow (and continuous) oxidation of the catechol species is undertaken (500 mV s^{-1} scan rate), E_{pa} shifts to more positive potential values with increasing ΔE_p (see Table 5) and the process probably becomes less reversible.[23] Such behaviour may only be explained by a short-lived reduced form which may suffer some type of adsorption process.[17]

For the negative potential range, typically at *ca.* -1.3 V, some reversible or irreversible redox waves can be assigned to processes centred on the π-conjugated pyridyl ligands (Table 5).[11–14,18,25]

Further topological considerations on the co-ordination mode of [12]aneS$_4$ in Ru(II) complexes

Table 6 lists the relevant structural parameters for the characterisation of the co-ordination modes of the [12]aneS$_4$ ligand in ruthenium(II) complexes. All compounds show a *cis*-octahedral environment with the equatorial plane determined by two macrocyclic sulfur and two other donor atoms from monodentate ligands (complexes **1–4**) or from a bidentate ligand (complexes **5–7** and **9–10**). To achieve this geometric arrangement the macrocyclic ligand folds significantly along a line defined by the axial sulfur donors. This folding can be easily characterised through the folding angle (Ω) defined as the dihedral angle between the two planes formed by the axial sulfur atoms and each equatorial sulfur atom (*e.g.* S(4), S(4*), S(1) and S(4), S(4*), S(7) in **1**, Fig. 1). In the polypyridylic complexes **6**, **7** and **9**, **10**, containing phen, bpy, 5,6-dione or dip ligands, the [12]aneS$_4$ macrocycle displays a pronounced folding with the Ω angle ranging from 58.6(1) to 59.8(1)°. A larger Ω angle of 81.6(1)° was seen for complex **5** containing the 5-phen ligand. Similar Ω angles were also reported for the complexes containing monodentate ligands: **1** 78.05(8), **2** 79.2(1), **3** 77.9(1) and **4** 77.1(1)°. The magnitude of the folding of the [12]aneS$_4$ macrocycle, in principle, should result from the minimisation of the steric interactions between the ligands present in the octahedral metal co-ordination sphere. However, the values found for the Ω angle suggest that there is no straightforward relationship between the folding of this macrocyclic ligand and the steric bulk of the ligands phen, bpy, dip, 5,6-dione or 5-phen or dmso–Cl, CH_3CN–Cl, CH_3CN–CH_3CN and Cl–ind.

The endocyclic torsion angles S–C–C–S, C–C–S–C and C–S–C–C, indicate that the macrocycle adopts, in all complexes, only two different conformations. The complexes **1–5** show a type I [*gtggttggtgtt*] conformation while the complexes **6**, **7**, **9** and **10** exhibit a type II [*ggggttggggtt*] conformation. For complex **2**, which is disordered, the macrocyclic conformation was determined using the macrocyclic atomic positions with major occupancy (0.591(2)). Furthermore it is clear that the Ω angle is related to the type of conformation adopted by the macrocyclic ligand. Thus, in the complexes containing monodentate ligands, **1–4**, the conformation of the macrocyclic ring is always of the type I and the Ω angle takes values between 77.2(1) and 79.2(1)°. Complex **5** containing the bidentate ligand 5-phen also retains a slightly distorted type I conformation with a Ω angle of 81.6(1)°. This conformation is also observed for *cis*-octahedral complexes [Rh([12]aneS$_4$)(phi)]$^{3+}$ **13**, where phi (9,10-phenanthrenequinone diimine) is also a bidentate ligand[27] and [Ni([12]aneS$_4$)Cl$_2$] **14**,[28] where the

Table 6 Comparison of the co-ordination mode of the [12]aneS$_4$ in ruthenium(II) complexes

	Bonds/Å		Angles/°		
Complex	Ru–S$_{eq}$	Ru–S$_{ax}$	S$_{ax}$–Ru–S$_{ax}$	Ω	Conformation[a]
[Ru([12]aneS$_4$)(dmso)Cl]$^+$ **1**	2.315(2)	2.367(3)	166.38(5)	78.05(8)	I
[Ru([12]aneS$_4$)(CH$_3$CN)$_2$]$^{2+}$ **2**	2.305(4)	2.363(2)	167.6(1)	79.2(1)	I
[Ru([12]aneS$_4$)(CH$_3$CN)Cl]$^+$ **3**	2.278(4)	2.356(2)	167.2(1)	77.9(1)	I
[Ru([12]aneS$_4$)(ind)Cl]$^+$ **4**	2.293(3)	2.358(3)	167.1(1)	77.1(1)	I
[Ru([12]aneS$_4$)(5-phen)]$^{2+}$ **5**	2.302(1)	2.360(1)	166.5(1)	81.6(1)	I
[Ru([12]aneS$_4$)(5,6-dione)]$^{2+}$ **10**	2.295(2)	2.382(2)	161.8(1)	59.8(1)	II
[Ru[12]aneS$_4$(dip)]$^{2+}$ **6**[b]	2.321(3)	2.400(3)	162.0(1)	58.6(1)	II
[Ru([12]aneS$_4$)(phen)]$^{2+}$ **7**[b]	2.316(3)	2.391(3)	161.9(1)	59.8(1)	II
[Ru([12]aneS$_4$)(bpy)]$^{2+}$ **9**[b]	2.309(2)	2.420(2)	162.5(2)	59.4(8)	II

[a] These two classifications were obtained from endocyclic torsion angles listed successively along the ring starting at the S–C–C–S angle. Those torsion angles which are greater or lesser than |120°| determine *trans* (*t*) or *gauche* (*g*) bonds respectively. I and II are the *gtggttggtgtt* and the *ggggttggggtt* conformations respectively. Both are called [2424] in the extended Dale nomenclature.[26] [b] Ref. 5.

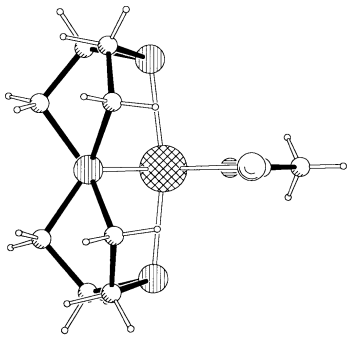

[Ru([12]aneS$_4$)(CH$_3$CN)Cl]$^+$ **3**

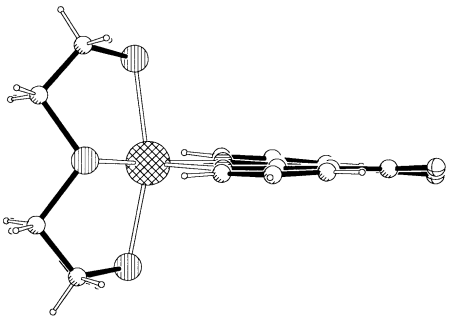

[Ru([12]aneS$_4$)(5,6-dione)]$^{2+}$ **10**

Fig. 9 Views of the [Ru([12]aneS$_4$)(CH$_3$CN)Cl]$^+$ **3** and [Ru([12]aneS$_4$)(5,6-dione)]$^{2+}$ **10** cations, parallels to the equatorial co-ordination plane, illustrating the two different conformations adopted by [12]aneS$_4$ in the ruthenium(II) complexes.

two nickel centres are bridged by two chlorine atoms in a centrosymmetric arrangement. The complexes **13** and **14** have Ω angles of 77.3 and 75.4° respectively. For bidentate complexes **6**, **7**, **9** and **10** the macrocyclic ligand displays a type II conformation and the Ω angle has more acute values between 58.6(1) and 59.8(1)°.

The two conformations discussed above are shown in Fig. 9 for complexes **10** and **3** respectively. In complexes **5–7** and **9**, **10** the two S–CH$_2$–CH$_2$–S moieties of the macrocyclic backbone are related approximately by a twofold axis defined by the intersection of the equatorial and the axial co-ordination planes. Complex **10** has C_2 symmetry imposed crystallographically. In complexes **1–4** these two units are related by the mirror plane comprising the equatorial donor atoms. In complexes **1** and **3** the mirror plane is imposed crystallographically.

In the conformational analysis of [12]aneS$_4$ in the gas phase, the two conformations found in these complexes differ only by 5.1 kJ mol^{-1}.[29] There are other low energy conformations but they are not suitable for metal distance and angle constraints imposed by the octahedral co-ordination in Ru(II), Rh(III) or Ni(II) centers. Therefore, these results indicate that both conformations can be adopted in the solid state, when the metal centre is co-ordinated by the [12]aneS$_4$ macrocycle in *cis*-octahedral geometric arrangement.

The conformation and consequently the folding exhibited by the macrocyclic ring, therefore, in our opinion, reflects the crystal packing effects rather than the presence of monodentate or bidentate bulky ligands, in the metal co-ordination sphere.

As has been reported[5] for complexes **6**, **7** and **9** and as is seen for the new complexes **1–5** and **10** the angle between the axial sulfur donor atoms and the ruthenium centre (S_{ax}–Ru–S_{ax}) is *ca.* 10° less than the expected value of 180° for an ideal octahedron. The small cavity size of the [12]aneS$_4$ ring, which precludes the axial sulfur atoms from achieving the ideal positions of a perfect octahedron, leads to reduced S_{ax}–Ru–S_{ax} angles. The Ru–S bond lengths are also determined by the small cavity size of the macrocyclic ligand. In complexes **3–7**, and **9**, **10**, the axial Ru–S bond lengths are significantly longer than the equatorial Ru–S bond lengths. In spite of the disorder seen for the macrocycle, complex **2** has an average axial Ru–S bond length [2.363(2) Å] which is slightly longer than the average equatorial Ru–S bond length [2.305(4) Å].

Experimental

General data

The ligands [12]aneS$_4$, dipa, 5-phen, pda, dbp and ind were purchased from the Aldrich Chemical Company and used without any further purification. The ligand 5,6-dione was synthesised according to a slightly modified experimental procedure taken from ref. 30.

The NMR spectra were recorded on either a Bruker AMX spectrometer operating at 300 MHz or a Bruker ARX spectrometer operating at 400 MHz. The ^{1}H spectra were obtained using 16k data points and a sweep width of 14.0 ppm. Deuteriated methanol, acetonitrile or D$_2$O were used as solvents with chemical shifts being referenced to HOD (δ 4.75), CD$_2$HOD (δ 3.35) or CD$_2$HCN (δ 1.94). ^{13}C spectra were recorded with a 260 ppm sweep width and 32k data points. Proton decoupling was carried out using WALTZ16.[37] The UV/Vis spectra were obtained at room temperature on a Jasco V-560 spectrophotometer in aqueous phosphate buffer or CH$_3$CN solutions. IR spectra were obtained as KBr pellets using a FTIR Mattson-7000 infrared spectrophotometer. Elemental analyses were obtained with a LECO CHNS-932 Elemental Analyser.

Electrochemical studies of the complexes were carried out on a BAS CV-50W-1000 voltammetric analyser. Cyclic voltammetric experiments were performed in a C-2 glass cell BAS-MF-1082, under nitrogen at room temperature with NBu$_4$PF$_6$ salt as the supporting electrolyte. The reference electrode was the Ag–Ag$^+$ couple, consisting of a CH$_3$CN solution of AgNO$_3$ in contact with a silver wire placed in glass tubing with a Vycor frit at one end to allow ion transport. Calibration was carried out against a ferrocene solution (1 mM). The Fc–Fc$^+$ couple *vs.* Ag–Ag$^+$ was found to occur with ΔE_p of 66 mV and $E_{1/2}$ of 89 mV. The auxiliary electrode was a Pt wire (Bas-MW-1032) and the working electrode a Pt disc (Bas-MF-2013) sealed in K-F plastic. Before and between each CV scan, whenever necessary, the working electrode was electrochemically cleaned, polished with diamond, 1 μm and 0.05 μm alumina, rinsed with CH$_3$CN and NBu$_4$PF$_6$ solution and finally sonicated, according to standard procedures. The CH$_3$CN was HPLC grade.

Synthesis of ruthenium(II) complexes

***cis*-[Ru(dmso)$_4$Cl$_2$].** The synthesis of the starting material *cis*-[Ru(dmso)$_4$Cl$_2$] was carried out according to the method of Evans *et al.*[31]

***cis*-[Ru([12]aneS$_4$)(dmso)Cl]Cl 1.** The thioether macrocycle [12]aneS$_4$ (241 mg; 1 mmol) was added to *cis*-[Ru(dmso)$_4$Cl$_2$] (485 mg; 1 mmol) in dearated absolute ethanol (15 ml). The resulting suspension was refluxed for 4 hours at 85 °C, under an argon atmosphere. During reflux the colour turned from pale to bright yellow. After cooling at room temperature, 10 ml of diethyl ether were added to the solution which was left at −20 °C until a bright yellow solid separated. The crystalline solid was filtered off, washed with cold diethyl ether and dried at 110 °C (415 mg, 85% yield) (Found: C, 24.0; H, 4.6; S, 32.5. Calc. for C$_{10}$H$_{22}$Cl$_2$ORuS$_5$: C, 24.5; H, 4.5; S, 32.7%). ^{1}H NMR (D$_2$O): δH 3.95 (2H, m),

3.45 (2H, m) 3.10–3.30 (4H, m; 6H, s) 2.96 (4H, m), 2.70 (4H, m). UV/Vis (H_2O) λ_{max} nm ($\varepsilon \times 10^{-3}$ M^{-1} cm^{-1}): 399 (0.9); 348 (0.4) sh; 214 (23.8). IR (KBr, cm^{-1}): 1076 vs and 1020 vs (ν(S=O), S co-ordinated), 447 m and 424 s (ν(Ru–S)), 378 s (δ(C–S–O)), 280 m (ν(Ru–Cl)). After replacing the Cl^- counter ion by PF_6^-, suitable crystals for single crystal X-ray analysis were obtained from a CH_3CN solution under a diethyl ether atmosphere.

[Ru([12]aneS$_4$)(CH$_3$CN)$_2$][PF$_6$]$_2$ 2. Complex **1** (74 mg; 0.15 mmol) and 105 mg (0.30 mmol) of $TlPF_6$ were mixed in dearated acetonitrile (10 ml) with immediate turbidity and kept under reflux at 80 °C for 10 hours with subsequent TlCl precipitation. The decanted solution was filtered, reduced in volume and, after diethyl ether addition, a light yellow solid precipitated. The solution was left at −20 °C for several hours, the solid filtered off and dried overnight (64 mg; 60% yield). Single crystals were obtained after dissolution in CH_3CN and standing under a diethyl ether atmosphere (Found: C, 20.48; H, 3.03; N, 4.01; S, 18.07. Calc. for $C_{12}H_{22}F_{12}N_2P_2RuS_4$: C, 20.20; H, 3.11; N, 3.93; S, 17.97%). ^{1}H NMR (CD_3CN): δH 4.01 (2H, dd), 3.57 (2H, dd), 3.39–3.30 (4H, m) and 2.98–2.58 (8H, m) (macrocycle), 2.42 (3H, s), 2.38 (3H, s) (co-ordinated CH_3CN). ^{13}C NMR (CD_3CN): δC 44.54, 40.86, 35.90 and 33.39 (macrocycle). UV/Vis (CH_3CN) λ_{max}/nm ($\varepsilon \times 10^{-3}$ M^{-1} cm^{-1}): 382 (1.7), 252 (2.4) sh, 211 (25.9). IR (KBr, cm^{-1}): 2322 w, 2289 w and 2254 w (ν(C=N)), 835 vs (PF_6^-), 558 vs (PF_6^-) and 443 w (ν(Ru–S)).

[Ru([12]aneS$_4$)(CH$_3$CN)Cl]PF$_6$ 3. Complex **1** (393 mg; 0.8 mmol) and an equimolar quantity of NH_4PF_6 were dissolved in CH_3CN (25 ml) at room temperature. The solution was filtered and passed through a QAE Sephadex A-25 column (Cl^- form) and eluted with CH_3CN. Slow recrystallisation of the eluted CH_3CN solution under a diethyl ether atmosphere afforded suitable crystals for X-ray diffraction studies (129 mg; 23% yield) (Found: C, 21.40; H, 3.22; N, 2.35; S, 23.30. Calc. for $C_{10}H_{19}ClF_6NPRuS_4$: C, 21.33; H, 3.40; N, 2.49; S, 22.78%). ^{1}H NMR (CD_3CN): δH 3.93 (2H, dd), 3.50 (2H, d), 3.33–3.19 (4H, m), 3.08 (2H, dd), 2.87–2.66 (6H, m) from macrocycle and 1.97 (3H, s). UV/Vis (CH_3CN) λ_{max}/nm ($\varepsilon \times 10^{-3}$ M^{-1} cm^{-1}): 406 (1.1), 271 (2.3) sh, 213 (27.4). IR (KBr, cm^{-1}): 2320 w and 2282 w (ν(C=N)), 839 vs (PF_6^-), 558 vs (PF_6^-), 440 w (ν(Ru–S)) and 266 m (ν(Ru–Cl)).

[Ru([12]aneS$_4$)(ind)Cl]PF$_6$ 4. An excess of ind (177 mg; 1.5 mmol) was added to 245 mg (0.5 mmol) of complex **1** and the mixture was refluxed for 13 hours. The PF_6^- salt of the compound was isolated as a yellow powder (279 mg; 87% yield). Deep orange crystals suitable for X-ray diffraction studies were developed by slow precipitation from a CH_3CN solution under a diethyl ether atmosphere (Found: C, 27.8; H, 3.5; N, 4.0; S, 20.0. Calc. for $C_{15}H_{22}ClF_6N_2PRuS_4$: C, 28.2; H, 3.5; N, 4.4; S, 20.0%). ^{1}H NMR (CD_3CN): δH 12.0 (1H, br), 8.34 (1H, s), 7.77 (1H, d), 7.67 (1H, d), 7.46 (1H, t), 7.23 (1H, t) 4.00 (2H, m), 3.50–3.10 (12H, m), 2.90 (2H, m). UV/Vis (phosphate buffer 0.1 M, pH 7.2) λ_{max}/nm ($\varepsilon \times 10^{-3}$ M^{-1} cm^{-1}): 405 (1.3), 307 (8.8) sh, 296 (9.1) sh, 290 (9.1), 247 (5.6) sh, 204 (48.4). IR (KBr, cm^{-1}): 3332 w and 3278 w (ν(N–H)), 1506 w (δ(N–H)), 842 vs (PF_6^-), 557 s (PF_6^-), 434 m (ν(Ru–S)), and 268 w (ν(Ru–Cl)).

[Ru([12]aneS$_4$)(5-phen)][PF$_6$]$_2$ 5. 128 mg (0.5 mmol) of 5-phen were added to complex **1** (245 mg, 0.5 mmol) in 15 ml of dearated ethanol and left under reflux (85 °C) for 10 hours. After cooling the stoichiometric addition of NH_4PF_6 was carried out. Bright yellow crystals were obtained by slow evaporation of the solvent (418 mg; 94% yield) (Found: C, 34.9; H, 3.0; N, 3.0; S, 14.3. Calc. for $C_{26}H_{28}F_{12}N_2P_2RuS_4$: C, 35.2; H, 3.2; N, 3.2; S, 14.5%). ^{1}H NMR (CD_3CN): δH 9.72 (2H, br), 8.75 (1H, d), 8.62 (1H, d), 8.22 (1H, s), 8.02 (2H, m), 7.65 (5H, s), 3.9–3.4 (8H, br), 2.97 (8H, br). UV/Vis (CH_3CN) λ_{max}/nm ($\varepsilon \times 10^{-3}$ M^{-1} cm^{-1}): 420 (7.2), 315 (8.3) sh, 281 (27.4), 239 (37.8), 204 (62.1), 195 (55.6) sh. IR (KBr, cm^{-1}): 837 vs (PF_6^-), 557 s (PF_6^-) and 465 w and 432 w (ν(Ru–S)).

[Ru([12]aneS$_4$)(dbp)][PF$_6$]$_2$ 8. 154 mg, (0.50 mmol) of dbp was added to 245 mg (0.50 mmol) of complex **1** in 15 ml of deaerated ethanol. The yellow mixture was refluxed for 10 hours at 85 °C and a dark brown solution was obtained. After cooling at room temperature, an equimolar quantity of NH_4PF_6 was added and a yellow-brown solid precipitated. After standing overnight at −20 °C the solid was filtered off and washed with cold water, cold ethanol and diethyl ether. The crude product was evaporated to dryness, redissolved in CH_3CN and put under a diethyl ether atmosphere until a bright yellow precipitate appeared. This solid was filtered off, successively washed with cold water, cold ethanol and diethyl ether and dried (245 mg; 52.2% yield) (Found: C, 37.90; H, 3.55; N, 2.84; S, 13.58. Calc. for $C_{30}H_{32}F_{12}N_2P_2RuS_4 \cdot 0.5H_2O$: C, 37.98; H, 3.51; N, 2.95; S, 13.52%). ^{1}H NMR (CD_3CN): δH 9.35 (2H, br), 8.94 (2H, s), 8.03–7.96 (6H, m), 7.63 (6H, m), 3.53 (8H, br), 2.93 (8H, br). UV/Vis (CH_3CN) λ_{max}/nm ($\varepsilon \times 10^{-3}$ M^{-1} cm^{-1}): 426 (7.3), 311 (20.7), 279 (33.3), 205 (53.2), 195 (72.9). IR (KBr, cm^{-1}): 837 s (PF_6^-), 557 m (PF_6^-) and 423 w (ν (Ru–S)).

[Ru([12]aneS$_4$)(5,6-dione)][PF$_6$]$_2$ 10. A slight excess of 5,6-dione (105 mg, 0.50 mmol) was added to 215 mg (0.43 mmol) of complex **1** in 20 ml of dearated ethanol. The yellow mixture was refluxed for 3 hours at 90 °C and a dark brown solution was obtained. The PF_6^- salt was prepared as green-brown solid needles (180 mg, 50% yield) (Found: C, 28,6; H, 2,5; N, 3.3. Calc. for $C_{20}H_{22}N_2O_2S_4P_2F_{12}Ru$: C, 28.5; H, 2.6; N, 3.3%. ^{1}H NMR (CD_3CN): δH 9.58 (2H, br), 8.69 (2H, d), 7.92 (2H, dd), 3.9–3.3 (8H, br), 2.96 (8H, br). UV/Vis (phosphate buffer 0.1 M, pH 7.2) λ_{max} nm ($\varepsilon \times 10^{-3}$ M^{-1} cm^{-1}): 410 (5.2), 325 (4.7) sh, 300 (12.4), 295 (12.5), 256 (12.8) sh, 200 (40.2). IR (KBr, cm^{-1}): 1699 s (ν(C=O)), 1308 m (δ(C–(C=O)–C)), 841 vs (PF_6^-), 559 s (PF_6^-) and 471 w and 420 w (ν(Ru–S)).

[Ru([12]aneS$_4$)(dipa)]Cl$_2$ 11. 171 mg (1.00 mmol) of dipa were added to 413 mg (0.85 mmol) of complex **1** in 20 ml of dearated ethanol. The yellow mixture was refluxed for 4 hours at 90 °C. After standing overnight a dark red-brown microcrystalline solid was obtained, which was washed with diethyl ether and dried under vacuum (130 mg, 26% yield) (Found: C, 36.7; H, 4.8; N, 7.0. Calc. for $C_{16}H_{21}N_3S_3F_6PClRu \cdot 0.5H_2O$: C, 36.5; H, 4.5; N, 7.1%). ^{1}H NMR (D_2O): δH 7.84 (2H, br), 7.61 (2H, t), 6.97 (2H, d), 6.87 (2H, t), 3.57, 3.19, 2.51 (br, 16H). UV/Vis (H_2O) λ_{max}/nm ($\varepsilon \times 10^{-3}$ M^{-1} cm^{-1}): 399 (0.86) sh, 320 (6.07) sh, 282 (13.64), 238.5 (13.70) sh, 193 (39.62). IR (KBr, cm^{-1}): 3329 m, 3255 m and 3215 m (ν(N–H)) and 1524 m (δ(N–H)).

[Ru([12]aneS$_4$)(pda)]Cl$_2$ 12. 54 mg (0.50 mmol) of pda were added to 245 mg (0.50 mmol) of complex **1** in 15 ml of dearated absolute ethanol. The solution was refluxed (85 °C) for 3 hours and a terracotta solid obtained. This solid was filtered off, washed with diethyl ether and dried (206 mg; 79% yield) (Found: C, 31.8; H, 4.3; N, 5.2. Calc. for $C_{14}H_{24}Cl_2N_2RuS_4$: C, 32.3; H, 4.6; N, 5.4%). ^{1}H NMR (D_2O): δH 7.18–7.08 (4H, m, aromatic H), 3.82 (2H, dd), 3.72 (2H, m), 3.32 (2H, dd), 3.17 (2H, m), 2.8–2.6 (6H, m), 2.35 (2H, m). UV/Vis (H_2O) λ_{max}/nm ($\varepsilon \times 10^{-3}$ M^{-1} cm^{-1}): 508 (0.4), 389 (1.2), 239 (4.3) sh, 206 (29.2) sh, 192 (40.9). IR (KBr, cm^{-1}): 3228 w (ν(N–H)), 1598 m (δ(N–H)), 929 m (γ(N–H)), 445 m (ν(Ru–S) overlaps with pda vibrations).

Table 7 Room temperature crystal data and refinement details for complexes **1–5** and **10**

	1	**2**	**3**	**4**	**5**	**10**
Empirical formula	$C_{10}H_{22}ClF_6ORuS_5$	$C_{12}H_{22}F_{12}N_2P_2RuS_4$	$C_{10}H_{19}ClF_6NPRuS_4$	$C_{15}H_{22}ClF_6N_2PRuS4 \cdot CH_3CN$	$C_{26}H_{28}F_{12}N_2P_2RuS_4$	$C_{20}H_{22}F_{12}N_2O_2P_2RuS_4 \cdot 2CH_3CN$
M	600.07	713.57	562.99	681.13	887.75	923.75
Crystal system	Orthorhombic	Monoclinic	Monoclinic	Orthorhombic	Orthorhombic	Monoclinic
Space group	*Pnma*	$P2_1/c$	*Cm*	$Pc2_1b$	*Pcab*	$C2/c$
a/Å	9.210(10)	10.391(11)	12.264(15)	7.655(9)	19.952(23)	18.893(20)
b/Å	9.779(11)	20.939(23)	9.189(11)	15.928(17)	14.860(16)	11.713(13)
c/Å	22.597(24)	11.488(13)	8.822(10)	21.475(23)	21.524(23)	15.908(18)
β/°	(90.0)	90.38(1)	96.02(1)	(90.0)	(90.0)	104.06(1)
Z	4	4	2	4	8	4
V	2035(4)	2499(5)	988(2)	2618(5)	6382(12)	3415(7)
D_c/g cm^{-3}	1.958	1.896	1.891	1.728	1.848	1.797
μ/mm^{-1}	1.544	1.184	1.479	1.136	0.948	0.895
F(000)	1200	1416	560	1368	3552	1848
Reflections measured	5303	4582	1642	7339	17142	4329
Unique reflections	1885(R_{int} = 0.0234)	4582(R_{int} = 0.0000)	1021(R_{int} = 0.0215)	4295(R_{int} = 0.0316)	5856(R_{int} = 0.0362)	2433(R_{int} = 0.0263)
R and $R_w[I > 2\sigma(I)]$	0.0271, 0.0798	0.0630, 0.1613	0.0439, 0.1246	0.0677, 0.1946	0.0516, 0.1306	0.0548, 0.1551
(all data)	0.0298, 0.0839	0.0814, 0.1713	0.0441, 0.1250	0.0881, 0.2202	0.0788, 0.1444	0.0628, 0.1644

Crystallography

Table 7 lists the crystal data and refinement details for complexes **1**–**5** and **10** respectively. The X-ray data for all six complexes were collected on a MARresearch image plate system using graphite Mo-Kα radiation (λ = 0.710 73 Å) at the University of Reading. The crystals were positioned at 70 mm from the image plate. 95 frames were measured at 2° intervals with a counting time adequate to the diffraction pattern exhibited by the crystal under study. Data analysis was carried out with the XDS program.[32] Intensities were not corrected for absorption effects.

The positions of the ruthenium atoms were retrieved from the three-dimensional Patterson maps and subsequent difference Fourier syntheses revealed the positions of the remaining non-hydrogen atoms.

The earliest difference maps calculated for complexes **3**, **4** and **10** show clearly that in both cases the fluorine atoms of the PF_6^- anions were disordered over two sites. Therefore, these anions were introduced in the refinement on two alternative positions with refined occupation factors for one major component of the disorder of 0.546(15) in **4** and 0.526(8) in **10**. For complex **3** an occupation factor of 0.5 was considered for two alternative positions.

The analysis of thermal parameters for complex **2** revealed that two sulfur atoms S(1) and S(7) and five carbon atoms C(8), C(6), C(2), C(12) and C(11) had high thermal parameters in one direction suggesting that these atoms were affected by some positional disorder. After many trial refinements, we found that the following disorder model gave the best fit to the electronic density map: the carbon atoms accompanied by their hydrogen atoms and two sulfurs were positioned on two alternative positions leading to two different conformations for the macrocyclic ligand (see above, Results and discussion). A refined value of 0.591(2) was obtained for the major disorder component.

All non-hydrogen atoms were refined with anisotropic parameters, except those that exhibited positional disorder, which were refined with isotropic parameters. The structures were refined against F^2 by full-matrix least-squares methods using a weighting scheme.

Structures were solved and refined using SHELXS and SHELXL within the SHELX97 package.[33] The molecular diagrams were drawn with the following graphical software packages XPMA and ZORTEP[34] and PLATON.[35]

CCDC reference number 440/135. See http://www.rsc.org/suppdata/nj/1999/1015/ for crystallographic files in .cif format.

Concluding remarks

We have reported the synthesis of new Ru^{II} [12]aneS_4 complexes containing bidentate polypyridylic or mondentate ligands from the starting material *cis*-[Ru([12]aneS_4)(dmso)Cl]$^+$. The synthesis of these complexes is a straightforward process, which is carried out under mild conditions. Furthermore, the Cl and dmso ligands in complex **1** display different labilities allowing selective replacement, of the dmso for other modentate ligands such as CH_3CN or ind, in the Ru(II) co-ordination sphere. Therefore, this synthetic approach has revealed an efficient pathway to produce Ru^{II}[12]aneS_4 complexes containing larger polypyridylic ring systems, which display recognised intercalative abilities, such as dppz (dppz = dipyrido[3,2-*a* : 2′,3′-*c*]phenazine).[36] All six complexes characterised by X-ray diffraction show a *cis*-octahedral geometric arrangement with the macrocyclic ligand adopting a folded strained conformation. In all studied complexes, the strain imposed by the macrocyclic ligand leads to smaller than expected S_{ax}–Ru–S_{ax} angles for ideal octahedral geometry. The same effect gives rise to Ru–S_{ax} bonds larger than their Ru–S_{eq} equivalents.

Acknowledgements

This work was supported by PRAXIS XXI, (PRAXIS/PCEX/C/QUI/122/96). V.F. acknowledges the Fundação de Ciência e Tecnologia and the British Council ("Acções Integradas" Programme) for a travel grant. The authors would also like to thank Helena Carapuça (University of Aveiro) for technical assistance with the electrochemistry. Finally, the authors are grateful to Professor Carlos Romão of the Instituto de Tecnologia Quimica e Biológica for fruitful discussions.

References

1 (*a*) M. R. Arkin, E. D. A. Stemp, R. E. Homlin, J. K. Barton, A. Hörmann, E. J. C. Olson and P. F. Barbara, *Science*, 1996, **273**, 475; (*b*) S. Arounaguiri and B. G. Maiya, *Inorg. Chem.*, 1996, **35**, 4267; (*c*) H. Mürner, B. A. Jackson and J. K. Barton, *Inorg. Chem.*, 1998, **37**, 3007; (*d*) P. J. Carter, C.-C. Cheng and H. H. Thorp, *J. Am. Chem. Soc.*, 1998, **120**, 632; (*e*) B. P. Hudson and J. K. Barton, *J. Am. Chem. Soc.*, 1998, **120**, 6877; (*f*) C. M. Dupureur and J. K. Barton, *Inorg. Chem.*, 1997, **36**, 33; (*g*) C. Turro, D. B. Hall, W. Chen, H. Zuilhof, J. K. Barton and N. J. Turro, *J. Phys. Chem. A*, 1998, **102**, 5708; (*h*) B. Nordén, P. Lincoln, B. Akerman and E. Tuite, in *Metal Ions in Biological Systems*, ed. A. H. Siegel, Marcel Dekker Inc., New York, 1996, vol. 33, p. 177; (*i*) J. G. Collins, A. D. Sleeman, J. R. Aldrich-Wright, I. Greguric and T. W. Hambley, *Inorg. Chem.*, 1998, **37**, 3133.

2 (*a*) M. Reed, K. Izatt, K. Pawlak and J. S. Bradshaw, *Chem. Rev.*, 1995, **95**, 2529; (*b*) K. P. Wainwright, *Coord. Chem. Rev.*, 1997, 35.
3 S. R. Cooper, S. C. Rawle, R. Yagbasan and D. J. Watkin, *J. Am. Chem. Soc.*, 1991, **113**, 1600.
4 B. J. Goodfellow, V. Félix, S. M. D. Pacheco, J. Pedrosa de Jesus and M. G. B. Drew, *Polyhedron*, 1997, **16**, 393.
5 B. J. Goodfellow, V. Félix, S. M. D. Pacheco, J. Pedrosa de Jesus, and M. G. B. Drew, *Polyhedron*, 1997, **16**, 3293.
6 C. Landgrafe and W. S. Sheldrick, *J. Chem. Soc., Dalton Trans.*, 1994, 1885.
7 J. E. Huheey, E. A. Keiter and R. L. Keiter, *Inorganic Chemistry, Principles of Structure and Reactivity*, Harper Collins College Publishers, New York, 4th edn., 1993, ch. 13, p. 547.
8 C. Tsiamis, R. Alberto, C. L. Barnes and S. Jurisson, *Inorg Chem.*, 1998, **37**, 2903.
9 B. J. Goodfellow and S. M. D. Pacheco, unpublished work.
10 M. J. Root, B. P. Sullivan, T. J. Meyer and E. Deutsh, *Inorg. Chem.*, 1985, **24**, 2731.
11 V. Balzani, A. Juris, M. Venturi, S. Campagna and S. Serroni, *Chem. Rev.*, 1996, **96**, 759.
12 G. Tresoldi, S. L. Schiavo, P. Piraino and P. Zanello, *J. Chem. Soc., Dalton Trans*, 1996, 885.
13 J.-Z. Wu, B.-H. Ye, L. Wang, L.-N. Ji, J.-Y. Zhou, R.-H. Li and Z.-Y. Zhou, *J. Chem. Soc., Dalton Trans.*, 1997, 1395.
14 B. J. Coe, S. Hayat, R. L. Bedoes, M. Helliwell, J. C. Jeffrey, S. R. Batten and P. S. White, *J. Chem. Soc., Dalton Trans.*, 1997, 591.
15 T. K. Misra, D. Das, C. Sinha, P. Ghosh and C. K. Pal, *Inorg. Chem.*, 1998, **37**, 1672.
16 D. P. Rillema and K. B. Mack, *Inorg. Chem.*, 1982, **21**, 3849; E. Garcia, J. Kwak and A. J. Bard, *Inorg. Chem.*, 1988, **27**, 4377.
17 E. Garcia, J. Kwak and A. J. Bard, *Inorg. Chem.*, 1988, **27**, 4377.
18 P. Ceroni, F. Paolucci, S. Roffia, S. Serroni and S. Campagna, *Inorg. Chem.*, 1998, **37**, 2829.
19 M. N. Ackermann and L. V. Interrante, *Inorg. Chem.*, 1984, **23**, 3904.
20 V. W.-W. Yam, V. W.-M. Lee and K.-K- Cheung, *J. Chem. Soc., Dalton Trans.*, 1997, 2335.
21 A. M. W. C. Thompson, D. A. Bardwell, J. C. Jeffery, L. H. Rees and M. D. Ward, *J. Chem. Soc., Dalton Trans.*, 1997, 721.
22 D. Sellmann, T. Gottschalk-Gaudig and F. W. Heinemann, *Inorg. Chim. Acta*, 1998, **269**, 63.
23 P. L. Hill, L. Y. Lee, T. R. Youkin, S. D. Orth and L. McElwee-White, *Inorg. Chem.*, 1997, **36**, 5655.
24 G. A. Fox, *Inorg. Chem.*, 1991, **30**, 2895.
25 K. J. Brewer, W. R. Murphy, Jr., S. R. Spurlin and J. D. Petersen, *Inorg. Chem.*, 1986, **25**, 882.
26 J. C. A. Boeyens and S. M. Robson, *Stereochemical and Stereophysical Behaviour of Macrocycles*, ed. I. Bernal, Elsevier, Amsterdam, 1987, vol. 2, 1, pp. 16–22.
27. A. H. Krotz, L. Y. Kuo, and J. K. Barton, *Inorg. Chem.*, 1993, **32**, 5963.
28 A. J. Blake, M. A. Halcrow and M. Schröder, *J. Chem. Soc., Dalton Trans.*, 1994, 1463.
29 V. Félix and M. G. B. Drew, unpublished work.
30 J. E. Dickeson and L. A. Summers, *Aust. J. Chem.*, 1970, **23**, 1023.
31 I. P. Evans, A. Spencer and G. Wilkinson, *J. Chem. Soc., Dalton Trans*, 1973, 204.
32 W. Kabsch, *J. Appl. Crystallogr.*, 1988, **21**, 916.
33 G. M. Sheldrick, SHELX-97, University of Göttingen, 1997.
34 L. Zsolnai, XPMA and ZORTEP, University of Heidelberg, 1994.
35 A. L. Spek, PLATON, A Multipurpose Crystallographic tool, Utrecht University, 1999.
36 (*a*) T. M. Santos, F. M. Amado, V. Félix, B. J. Goodfellow, J. P. de Jesus and M. G. B. Drew, *4th Biological Inorganic Chemistry Conference*, 1998, Seville, Book of Abstracts MM-61, 20–21; (*b*) R. E. Holmlin, E. D. A. Stemp and J. K. Barton, *Inorg. Chem.*, 1998, **37**, 29.
37 A. J. Shaka, J. Keeler and R. Freeman, *J. Magn. Res.*, 1983, **53**, 313.

Paper 9/03117K